INTERNATIONAL JOURNAL OF HYDROGEN ENERGY XXX (XXXX) XXX

Available online at www.sciencedirect.com

ScienceDirect

journal homepage: www.elsevier.com/locate/he

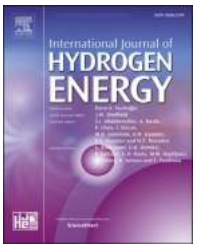

Performance assessment and optimization of a biomass-based solid oxide fuel cell and micro gas turbine system integrated with an organic Rankine cycle

Mohammad Hossein Karimi [a], *Nazanin Chitgar* [b], *Mohammad Ali Emadi* [b], *Pouria Ahmadi* [c,*], *Marc A. Rosen* [d]

[a] *Faculty of Mechanical Engineering, University of Guilan, Rasht, Iran*
[b] *School of Mechanical Engineering, Iran University of Science and Technology, Tehran 16844, Iran*
[c] *School of Mechanical Engineering, College of Engineering, University of Tehran, Tehran, Iran*
[d] *Faculty of Engineering and Applied Science, University of Ontario Institute of Technology, 2000 Simcoe Street North, Oshawa, ON, L1G 0C5, Canada*

HIGHLIGHTS

- A system driven by a SOFC is proposed for electricity generation and heating.
- Effects of key parameters on system performance are examined.
- The optimum working condition is obtained by multi-objective optimization.
- The optimum system generates 329 kW electricity and 56 kW heating.
- The exergy efficiency and total cost rate of the system are 35.1% and 10.2 $/h.

GRAPHICAL ABSTRACT

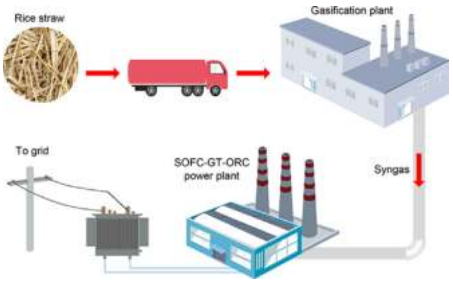

ARTICLE INFO

Article history:
Received 7 June 2019
Received in revised form
19 December 2019
Accepted 20 December 2019
Available online xxx

ABSTRACT

Rice straw is a potential energy source for power generation. Here, a biomass-based combined heat and power plant integrating a downdraft gasifier, a solid oxide fuel cell, a micro gas turbine and an organic Rankine cycle is investigated. Energy, exergy, and economic analyses and multi-objective optimization of the proposed system are performed. A parametric analysis is carried out to understand the effects on system performance and cost of varying key parameters: current density, fuel utilization factor, operating pressure, pinch point temperature, recuperator effectiveness and compressors isentropic efficiency. The results show that current density plays the most important role in achieving a tradeoff

* *Corresponding author.*
E-mail addresses: mohammadali_emadi@alumni.iust.ac.ir (M.A. Emadi), Pahmadi@ut.ac.ir (P. Ahmadi).
https://doi.org/10.1016/j.ijhydene.2019.12.143

Keywords:
Gasification
Multi-objective optimization
Solid oxide fuel cell (SOFC)
Micro gas turbine
Organic Rankine cycle (ORC)

between system exergy efficiency and cost rate. Also, it is observed that the highest exergy destruction occurs in the gasifier, so improving the performance of this component can considerably reduce the system irreversibility. At the optimum point, the system generates 329 kW of electricity and 56 kW of heating with an exergy efficiency of 35.1% and a cost rate of 10.2 $/h. The capability of this system for using Iran rice straw produced in one year is evaluated as a case study, and it is shown that the proposed system can generate 6660 GWh electrical energy and 1140 GWh thermal energy.

Nomenclature

A_{act}	Surface area (m^2)
CRF	Capital recovery factor
$\dot{C}$	Cost rate ($/hr)
ex	Specific exergy (kJ/kg)
$\dot{Ex}$	Exergy rate (kW)
$\overline{\Delta g^0}$	Change in Gibbs free energy (kJ/kmol)
$\overline{h}$	Molar enthalpy (kJ/kmol)
i	Current density (A/m^2)
K	Equilibrium constant
l	Thickness (m)
$\dot{m}$	Mass flow rate (kg/s)
N_{cell}	Number of fuel cells
$\dot{n}$	Molar flow rate (mol/s)
P	Pressure (bar)
$\dot{Q}$	Heat transfer rate (kW)
$\overline{R}$	Universal gas constant (8.314 kJ/kmol K)
$\overline{s}$	Molar entropy (kJ/kmol)
T	Temperature (K)
U_f	Fuel utilization factor
V	Voltage (V)
$\dot{W}$	Power (kW)
Z	Capital cost of a component ($)
$\dot{Z}$	Capital cost rate ($/hr)

Greek symbols

ζ	Voltage loss (V)
η_{ex}	Exergy efficiency (%)
ρ	Electrical resistivity of cell components, (Ω m)

Subscripts

0	Environmental condition
a	Anode
act	Activation
AB	Afterburner
AC	Air compressor
c	Cathode
ch	Chemical
conc	Concentration
Con	Condenser
CW	Cooling water
DH	District heating
DHW	Distrcit heating water
e	Electrolyte
ex	Exergy
Eva	Evaporator
G	Exhaust gas
in	Inlet
int	Interconnect
MGT	Micro gas turbine
N	Nernst
ohm	Ohmic
out	Outlet
ph	Physical
P	Pump
tot	Total
T	Turbine

Abbreviations

CHP	Combine heat and power
GT	Gas turbine
HRVG	Heat recovery vapor generator
ORC	Organic Rankine cycle
PPTD	Pinch point temperature difference
SOFC	Solid oxide fuel cell

Introduction

Population and economic growth are expected to drive increasing energy demands for decades [1]. Simultaneously, limited fossil fuel sources and their subsequent environmental issues have increased the importance of renewable energy [2]. With many government incentive programs, the growth rate of renewable energy use has become higher than that of other energy sources in many countries. Biomass (such as wood, agricultural residue, and municipal waste) with its renewability and worldwide availability is expected by many to play a key role in future energy scenarios [3].

Rice straw is a by-product of rice harvesting and can be utilized as a biomass resource. The world annual production of rice straw is about 731 million tons [4]. Due to an unawareness of uses of rice straw and also obstacles in gathering this bulky agricultural residue, notable amounts of rice straw are burnt on fields by farmers. This leads to emissions of greenhouse gases like CH_4, CO_2 and N_2O and thus causes environmental problems. Approximately half of the rice straw use is for rural and industrial purposes, while the remainder is burnt in fields [5]. Therefore, collecting and using rice straw as a biomass feedstock can be a means to retain its benefits and to reduce environmental impacts.

Please cite this article as: Karimi MH et al., Performance assessment and optimization of a biomass-based solid oxide fuel cell and micro gas turbine system integrated with an organic Rankine cycle, International Journal of Hydrogen Energy, https://doi.org/10.1016/j.ijhydene.2019.12.143

One approach to harvest the energy stored in biomass resources effectively is to convert it into a liquid or gaseous medium, which is easier to handle, store and transport [3]. This goal can be achieved through thermo-chemical conversion (i.e. pyrolysis, gasification, hydrothermal processing and liquefaction) or biochemical conversion (i.e. anaerobic digestion and fermentation). Gasification as a mature technology can be used to convert biomass into gaseous products (so called syngas), which mainly consist of H_2, CO, CH_4, CO_2, N_2, water vapor, and contaminants [6]. Nowadays, syngas combustion in externally fired gas turbines and engines is a common method for power generation. Recently, researchers have shown an increased interest in using syngas in fuel cells.

Solid oxide fuel cells (SOFCs) are promising devices that generate electrical current based on electrochemical conversion of fuels, with low environmental emissions and exergy losses. One advantage of SOFCs is that their exhaust gas has a high temperature that can be used for heating purposes or can be expanded through a micro gas turbine (MGT) to generate additional electricity [7]. Moller and Rokni [8] reported that a SOFC-MGT combination has higher electrical and exergy efficiencies as power generation unit than each device alone. If the syngas is cleaned to a sufficient level, it can be fed to the SOFC for electricity generation which leads to a biomass-based power generation system. Therefore, the integration of biomass gasification with a SOFC provides a promising option for biomass-based combined heat and power applications. A preliminary study of a biomass gasification and SOFC hybrid system was performed by Alderucci et al. [9]. The system was thermodynamically analyzed at several gasification conditions. They reported electrical efficiencies of 47% (with steam as the gasifying agent) and 51% (with CO_2 as the gasifying agent). Omosun et al. [10] investigated the efficiency and cost of two biomass fueled SOFC systems. One system involves cold gas cleaning and the other hot gas cleaning. It was shown that hot gas cleaning has a higher system efficiency while the cold process produces cleaner gas. Bang-Moller et al. [14] evaluated the feasibility of combining a biomass gasifier with SOFC and/or MGT in a small scale combined heat and power (CHP) plant. It was observed that the gasifier–SOFC–MGT hybrid system yields a higher electrical efficiency (η_{el} = 50.3%) than the gasifier-SOFC (η_{el} = 36.4%) and the gasifier-MGT (η_{el} = 28.1%) configurations. A biomass fueled SOFC-Stirling CHP plant was presented by Rokni [15]. He found that adding a Stirling engine to the SOFC plant improves the plant electrical efficiency by 29%. Morandin et al. [16] performed a thermo-economic optimization of several configurations of a wood-gasifier-SOFC system. They showed that the biomass gasifier-SOFC power generation system can achieve high efficiency but also is more expensive than other biomass based power generating systems. In one of the considered configurations, an efficiency of 65% and total investment cost about $450,000 (based on 2010 dollars) were reported for a nominal power of 60 kW.

An organic Rankine cycle (ORC) is often appropriate for power generation from waste heat of industrial units, especially where the heat source is low or medium grade [11,17,18]. Combining a SOFC with an ORC can be an option for improving resource recovery and increasing energy efficiency. Pierobon et al. [19] combined a biomass gasification system, a SOFC and an organic Rankine cycle. In that system, syngas obtained by woodchip gasification was fed to the SOFC and heat was recovered from the exhaust gas by an ORC for electricity generation. Also the optimal working fluid and ORC turbine inlet pressure were selected using a genetic algorithm. In that study, the electrical efficiency was calculated to be 54–56%. Yan et al. [20] performed a thermodynamic analysis of an SOFC-GT-ORC integrated power system with liquefied natural gas as a heat sink. Their study revealed that an electrical efficiency of 67% could be achieved for the system. Ebrahimi and Moradpoor [21] considered a micro scale CHP system consisting of a SOFC, a micro gas turbine and an organic Rankine cycle. The system's performance was investigated through a parametric analysis and it was concluded that the system is able to reduce fuel usage by about 45% compared to conventional power plants (with an efficiency of 30%) and to attain an overall efficiency of greater than 65%. In 2016, a hybrid power generation system with a SOFC, a gas turbine and an ORC was studied thermodynamically and economically by Eveloy et al. [22]. Six working fluids were examined and toluene was found to be the best for ORC performance. It was observed that the system exhibited an efficiency about 34% higher than that of a gas turbine cycle and about 6% higher than that of a SOFC-GT system. Also they demonstrated that the system could be profitable within three to six years. Tan et al. [23] used a Kalina cycle as a bottoming cycle for a power generation system integrating biomass gasification, a SOFC and a gas expander, and containing a CO_2 capture unit. They modeled the system thermodynamically and investigated its energy and exergy aspects. The results showed that utilizing waste heat in the Kalina cycle increases the energy efficiency by 10.3%.

Iran is a west Asian country with a population of over 80 million, where rice is a staple food. In this country rice is cultivated from about 600 ha in almost 20 provinces. According to the Iran Ministry of Agriculture [24], during the last decade, on average about 2.5 million tons of rice was produced annually in Iran and, since each ton of rice yields about 1.25 ton of rice straw [25], about 3.12 million tons of rice straw is produced in Iran annually. The aim of this work is to consider the possibility of using Iran's rice straw for power generation. For this purpose, a combined heat and power system is investigated which consists of a downdraft biomass gasifier that converts the rice straw to syngas, a solid oxide fuel cell that uses this syngas through an electrochemical reaction and produces electricity and heat as by-product, a micro gas turbine that expands the SOFC outlet stream for power generation, and finally an ORC that utilizes MGT mid-temperature exhaust gases and produces extra power. Also the system contains a cold gas cleaning process through which hot water for district heating applications is provided. To the authors' knowledge, this configuration has not been studied previously for biomass-based power generation. A comprehensive system investigation is performed which includes a parametric analysis, energy, exergy and economic analyses and a multi-objective optimization for minimizing the total cost rate while maximizing the exergy efficiency. Moreover, the performance of the proposed hybrid system is compared with the conventional Gasifier + SOFC-based system. In this comparison, the performance of the proposed hybrid system is

Please cite this article as: Karimi MH et al., Performance assessment and optimization of a biomass-based solid oxide fuel cell and micro gas turbine system integrated with an organic Rankine cycle, International Journal of Hydrogen Energy, https://doi.org/10.1016/j.ijhydene.2019.12.143

investigated from energy, exergy and economic perspectives. The optimized system is used to estimate the amount of power generation from Iran rice straw. Then the system output energy is compared with the energy needed for collecting rice straw from fields in order to demonstrate the potential advantages of the proposed system for power generation from rice straw.

System description

The system layout is shown in Fig. 1, which illustrates a biomass-fueled system containing a biomass gasifier, a SOFC, a MGT and an ORC cycle to generate electricity and heat as a by-product. The operation of the system can be described as follows. Biomass and air (point 1) enter an atmospheric downdraft gasifier. A syngas from gasification (point 2) passes through a cyclone which removes its large particulates (above $5\mu m$). In order to meet the impurity tolerance of the SOFC, further gas clean-up is necessary. For this purpose, a cold-gas cleaning process is performed in this plant. As step one in this process, the temperature of the hot syngas is reduced to 90 °C, which causes alkali compounds to condense on suspended particulates in the stream. The heat released in this step is recovered in the syngas preheater and the district heating system. Then the cooled gas is passed through a filter and a scrubber in order to remove the remaining particulates and tars. At this point (7), the clean stream is pressurized by the syngas compressor (SC) and is then preheated in the syngas preheater. Since chemical reactions occurring in the SOFC need steam as a reactant, the fuel (point 9) is merged in the mixer with recirculated anode outlet gas that is rich in steam. At the same time, air (point 19) is compressed and, after being preheated by passing through the recuperator and air preheater, is sent to the cathode side.

Then the electrochemical reaction occurs inside the SOFC, yielding a significant amount of electricity and heat. Before exiting the module, the anode outlet gas and the excess air from the cathode are mixed in the afterburner where unreacted fuel is combusted to preheat the incoming air. Next,

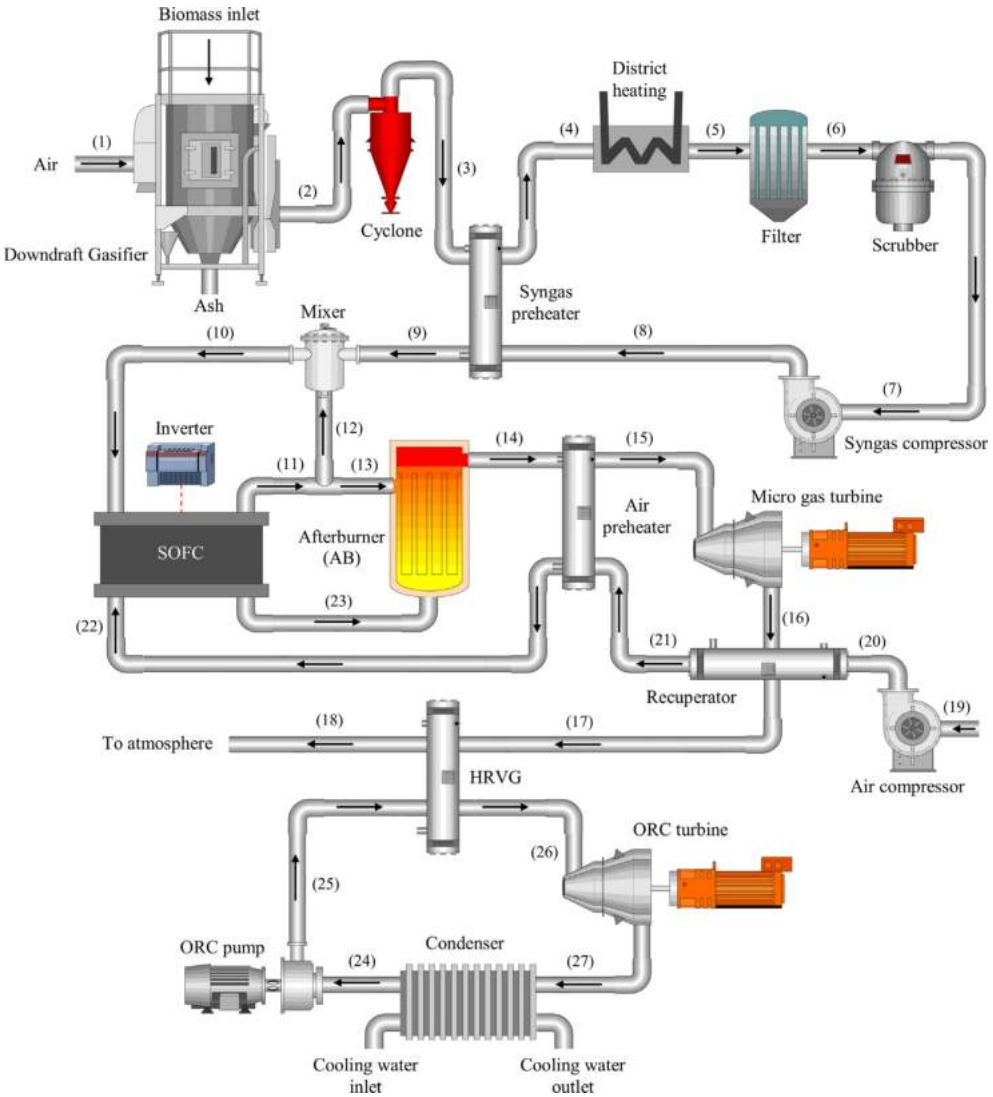

Fig. 1 – Schematic of the proposed system.

Please cite this article as: Karimi MH et al., Performance assessment and optimization of a biomass-based solid oxide fuel cell and micro gas turbine system integrated with an organic Rankine cycle, International Journal of Hydrogen Energy, https://doi.org/10.1016/j.ijhydene.2019.12.143

combustion products (point 15) are expanded through a micro gas turbine (MGT) where further power is extracted. Even though part of the energy from the turbine exhaust gas is utilized in the recuperator, it still has enough thermal energy to be used to produce vapor in a heat exchanger (specifically a HRVG) for the organic Rankine cycle. Cyclohexane is selected as the working fluid in the ORC, which is a dry fluid that becomes superheated during expansion from the vapor state, so superheating is not imperative. In the ORC, vapor (point 26) is expanded through the turbine to generate electrical power, and then returns to the initial state by rejecting heat in the condenser before being pumped to the HRVG pressure.

Plant modeling and analysis

The modeling of the plant is carried out in Engineering Equation Solver (EES) software. Heat losses in the pipes and devices are assumed to be zero and all components are considered to operate at steady state. The following subsections present thermodynamic models for each component.

Gasifier

A thermodynamic equilibrium method based on a stoichiometric approach is used for modelling the gasifier. This model is used to predict the syngas composition at the gasifier working temperature and pressure. The gasification global reaction can be written as [26]:

$$CH_aO_bN_c + w\ H_2O + m\ (O_2 + 3.76\ N_2) \rightarrow\ n_{H2}H_2 + n_{CO}CO + n_{CO2}CO_2 + n_{H2O}H_2O + n_{CH4}CH_4 + n_{N2}N_2 \quad (1)$$

Here, $CH_aO_bN_c$ is the general chemical formula of biomass based on its elemental analysis and w is the moisture content in the feedstock. In this case, a, b and c are determined according to the elemental analysis of the Iranian rice straw, as given in Table 1. By knowing the amount of inlet air (m) and the gasifier temperature (T_g) six equations are required to calculate the values of n_{H2}, n_{CO}, n_{CO2}, n_{H2O}, n_{CH4}, and n_{N2}. Four of these equations are obtained by balancing each of the atomic species in Eq. (1) as follows:

$$\text{Carbon balance}: \ n_{CO} + n_{CO2} + n_{CH4} = 1 \quad (2)$$

$$\text{Hydrogen balance}: \ 2n_{H2} + 2n_{H2O} + 4n_{CH4} = a + 2w \quad (3)$$

$$\text{Oxygen balance}: \ n_{CO} + 2n_{CO2} + n_{H2O} = b + w + 2m \quad (4)$$

$$\text{Nitrogen balance}: \ 2n_{N2} = c + 3.76 \times 2m \quad (5)$$

Table 1 – Iran rice straw ultimate analysis [27].

Element	Percentage (%)
C	49.70
H	5.88
N	1.10
S	0.06
O	40.60
Ash	2.66

Since oxidation reactions in the gasifier almost achieve an equilibrium state, by considering their equilibrium constant expression the secondary gas phase reactions can be derived. These reactions are:

$$C + 2H_2 \leftrightarrow CH_4 \quad \text{Methane reaction} \quad (6)$$

$$CO + H_2O \leftrightarrow CO_2 + H_2 \quad \text{Water} - \text{gas shift reaction} \quad (7)$$

Their equilibrium constants are:

$$K_{MR} = \frac{n_{CH4} \times n_{tot}}{(n_{H2})^2} = \exp\left(\frac{-\Delta G^0{}_{MR}}{RT_g}\right) \quad (8)$$

$$K_{SR} = \frac{n_{CO2} \times n_{H2}}{n_{CO} \times n_{H2O}} = \exp\left(\frac{-\Delta G^0{}_{SR}}{RT_g}\right) \quad (9)$$

where $\Delta G^0{}_{MR}$ and $\Delta G^0{}_{SR}$ are the change in the standard Gibbs free energy of the corresponding reactions, and R is the gas constant.

Solid oxide fuel cell

The capability of the SOFC system to use hydrogen and carbon monoxide as a fuel is an important advantage. The fuel cell can provide the required hydrogen from a variety of hydrocarbon fuels through an external or internal reformer. The SOFC's internal reformer which is supplied with syngas is less costly compared to the external type; moreover, no excess air is required for cooling the SOFC stack. The following assumptions are considered in SOFC modeling:

- Fuel cell operates under steady state conditions and the chemical reactions are at equilibrium.
- The entering air of the SOFC cathode is composed of 21% O2 and 79% N2.
- Unreacted gases are fully oxidised in the afterburner.
- There is no heat transfer between the system and the environment.

The output gas from the gasifier contains primarily methane. This methane is reformed completely to hydrogen and carbon dioxide thorough the reforming and shifting reactions (Eq. (10) and Eq. (11)). Simultaneously, the H_2 produced in this step is consumed in the fuel cell's electrochemical reaction (Eq. (12)).

$$\dot{x} \rightarrow [CH_4 + H_2O \ \leftrightarrow CO + 3H_2] \quad \text{Reforming} \quad (10)$$

$$\dot{y} \rightarrow [CO + H_2O \leftrightarrow CO_2 + H_2] \quad \text{Shifting} \quad (11)$$

$$\dot{z} \rightarrow \left[H_2 + \frac{1}{2}O_2 \rightarrow H_2O\right] \quad \text{Overall electrochemical reaction} \quad (12)$$

where $\dot{x}$, $\dot{y}$ and $\dot{z}$, respectively, are molar conversions of reactions. These variables can be calculated by simultaneously solving the equilibrium constants and fuel utilization factor (U_f). These equations can be written as follows:

Please cite this article as: Karimi MH et al., Performance assessment and optimization of a biomass-based solid oxide fuel cell and micro gas turbine system integrated with an organic Rankine cycle, International Journal of Hydrogen Energy, https://doi.org/10.1016/j.ijhydene.2019.12.143

$$K_{p,shift}=\frac{P_{CO2}P_{H2}}{P_{CO}P_{H2O}}=\frac{(\dot{n}_{CO2,in}+\dot{y})(\dot{n}_{H2,in}+3\dot{x}+\dot{y}-\dot{z})}{(\dot{n}_{CO,in}+\dot{x}+\dot{y})(\dot{n}_{H2O,in}-\dot{x}-\dot{y}+\dot{z})}=exp\left(\frac{\Delta\overline{g}^{0}_{shift}}{RT_{cell}}\right) \quad (13)$$

$$U_f=\frac{\dot{z}}{3\dot{x}+\dot{y}} \quad (14)$$

$$i=\frac{2.F.\dot{z}}{N_{cell}.A_{act}} \quad (15)$$

In this relation, P and $\dot{n}$ are respectively the partial pressure and molar rate of species, $\Delta\overline{g}^{0}_{shift}$, R, F, i, and T_{cell} are the Gibbs free energy, the universal gas constant, Faraday constant (9.649×10^7 C/kmol), current density and the output temperature from the fuel cell. The Gibbs free energy associated with the shifting reaction and the corresponding molar enthalpy and entropy changes can be written as follows:

$$\Delta\overline{g}^{0}_{shift}=\Delta\overline{h}_{shift}-T_{cell}\Delta\overline{s}_{shift} \quad (16)$$

$$\Delta\overline{h}_{shift}=\overline{h}_{H_2}+\overline{h}_{CO_2}-\overline{h}_{CO}-\overline{h}_{H_2O} \quad (17)$$

$$\Delta\overline{s}_{shift}=\overline{s}_{H_2}+\overline{s}_{CO_2}-\overline{s}_{CO}-\overline{s}_{H_2O} \quad (18)$$

In these relations, $\overline{h}$ and $\overline{s}$ are enthalpy and entropy per unit of mole.

The net electricity production rate via the SOFC stack is obtained as follows:

$$\dot{W}_{SOFC,stack}=i.A_{act}.N_{cell}.V_{cell} \quad (19)$$

The fuel cell voltage is derived as:

$$V_{cell}=V_N-V_{loss} \quad (20)$$

Here, V_N and V_{loss} are the cell reversible voltage and the sum of the Ohmic, activation and concentration overvoltages, respectively. That is,

$$V_{loss}=\zeta_{ohm}+\zeta_{act}+\zeta_{conc} \quad (21)$$

Expressions for the Nernst voltage, the overvoltages and the required constants are provided in Tables 2 and 3.

Organic Rankine cycle

In order to analyze the performance of the ORC from the perspective of the first law of thermodynamics, each device is regarded as a control volume, and the principles of mass and energy conservation are applied. In the steady state condition for a control volume, the principle of energy conservation can be expressed as:

$$\dot{Q}+\sum\dot{m}_i h_i=\dot{W}+\sum\dot{m}_o h_o \quad (36)$$

The equations used in modeling the ORC system are presented in Table 4.

Table 2 – Electrochemical equations.

Term	Equation	Eq. number
Nernst voltage	$V_N=\left(-\frac{\overline{\Delta g}^{\circ}_{s}}{n_eF}\right)-\frac{\overline{R}T_{cell}}{n_eF}\ln\left(\frac{P_{H_2O}}{P_{H_2}\sqrt{P_{O_2}}}\right)$	(22)
Ohmic overvoltage	$\zeta_{ohm}=(\rho_a l_a+\rho_c l_c+\rho_e l_e+\rho_{int} l_{int})i$	(23)
	$\rho_a=\left(\frac{95\times10^6}{T_{cell}}\exp\left(\frac{-1150}{T_{cell}}\right)\right)^{-1}$	(24)
	$\rho_c=\left(\frac{42\times10^6}{T_{cell}}\exp\left(\frac{-1200}{T_{cell}}\right)\right)^{-1}$	(25)
	$\rho_e=\left(3.34\times10^4\exp\left(\frac{-10300}{T_{cell}}\right)\right)^{-1}$	(26)
	$\rho_{int}=\left(\frac{9.3\times10^6}{T_{cell}}\exp\left(\frac{-1100}{T_{cell}}\right)\right)^{-1}$	(27)
Activation overvoltage	$\zeta_{act}=\zeta_{act,a}+\zeta_{act,c}$	(28)
	$\zeta_{act,a}=\frac{\overline{R}T_{cell}}{F}\left(Sinh^{-1}\left(\frac{i}{2i_{oa}}\right)\right)$	(29)
	$\zeta_{act,c}=\frac{\overline{R}T_{cell}}{F}\left(Sinh^{-1}\left(\frac{i}{2i_{oc}}\right)\right)$	(30)
Concentration overvoltage	$\zeta_{conc}=\zeta_{conc,a}+\zeta_{conc,c}$	(31)
	$\zeta_{conc,a}=\frac{-\overline{R}T_{cell}}{2F}\left(\ln\left(1-\frac{i}{i_{as}}\right)-\ln\left(1-\frac{P_{H_2}i}{P_{H_2O}i_{as}}\right)\right)$	(32)
	$\zeta_{conc,c}=\frac{-\overline{R}T_{cell}}{4F}\left(\ln\left(1-\frac{i}{i_{cs}}\right)\right)$	(33)
	$i_{as}=\frac{4FP_{H_2}D_{aeff}}{\overline{R}T_{cell}l_a}$	(34)
	$i_{cs}=\frac{4FP_{O_2}D_{ceff}}{\overline{R}T_{cell}l_c\left(1-\frac{P_{O_2}}{P_0}\right)}$	(35)

Table 3 – Constant parameters for voltage losses.

Parameter	Symbol	Value
Anode thickness (m)	l_a	0.05×10^{-2}
Cathode thickness (m)	l_c	0.005×10^{-2}
Electrolyte thickness (m)	l_e	0.001×10^{-2}
Interconnect thickness (m)	l_{int}	0.3×10^{-2}
Anode's effective diffusivity (m^2/s)	D_{aeff}	0.2×10^{-4}
Cathode's effective diffusivity (m^2/s)	D_{ceff}	0.05×10^{-4}
Exchange current density of anode (A/m^2)	i_{oa}	6500
Exchange current density of cathode (A/m^2)	i_{oc}	2500

Table 4 – Energy rate balance equations for components of the ORC.

Component	Equation
Turbine	$\dot{W}_{T,ORC}=\dot{m}_{ORC}(h_{26}-h_{27})$, $\eta_T=(h_{26}-h_{27})/(h_{26}-h_{27,is})$
Evaporator	$\dot{Q}_{Eva,ORC}=\dot{m}_G(h_{17}-h_{18})=\dot{m}_{ORC}(h_{26}-h_{25})$
Pump	$\dot{W}_{P,ORC}=\dot{m}_{ORC}(h_{25}-h_{24})$, $\eta_P=(h_{25,is}-h_{24})/(h_{25}-h_{24})$
Condenser	$\dot{Q}_{Con,ORC}=\dot{m}_{ORC}(h_{27}-h_{24})=\dot{m}_W(h_{out}-h_{in})$

Please cite this article as: Karimi MH et al., Performance assessment and optimization of a biomass-based solid oxide fuel cell and micro gas turbine system integrated with an organic Rankine cycle, International Journal of Hydrogen Energy, https://doi.org/10.1016/j.ijhydene.2019.12.143

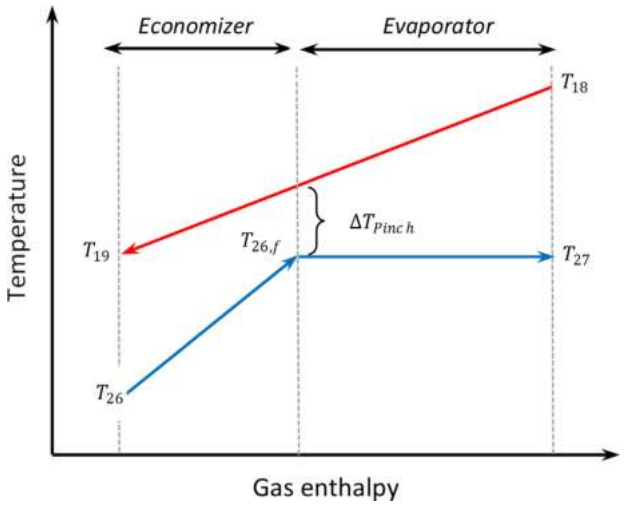

Fig. 2 – Temperature-enthalpy diagram of HRVG.

Heat exchangers

All heat exchangers in the system are of the counter flow type, for which the design parameters are calculated based on the $\varepsilon - NTU$ method:

$$\varepsilon = \frac{C_{hot}\left(T_{hot,\,in} - T_{hot,out}\right)}{C_{min}\left(T_{hot,in} - T_{cold,in}\right)} \tag{37}$$

Assuming no heat transfer to or from the environment:

$$\dot{n}_{in,hot}\left(\overline{h}_{in,hot} - \overline{h}_{out,hot}\right) = \dot{n}_{out,cold}\left(\overline{h}_{out,cold} - \overline{h}_{in,cold}\right) \tag{38}$$

The heat recovery is modeled using the pinch point temperature difference (ΔT_{pinch}) as illustrated in Fig. 2. The pinch point temperature is a critical parameter in heat exchanger design [28].

Exergy analysis

Energy analysis provides incomplete information about the quality of energy and of conversion processes for it. With exergy analysis, it becomes clear how efficient a system is for converting energy.

In this article, the chemical exergy rate of biomass, as the system inlet exergy, is computed as follows [29]:

$$\dot{E}x_{biomass} = \beta\left(LHV + wh_{fg}\right) \tag{39}$$

$$\beta = \frac{1.0438 + 0.1882(H/C) - 0.2509(1 + 0.7256(H/C) + 0.0383(N/C)}{1 - 0.3035(O/C)} \tag{40}$$

Here, LHV is the biomass heating value and H, C, O and N denote the molar fractions of each element, while w is the percent of moisture in the biomass. Also, β denotes the ratio of the chemical exergy to the low heating value (LHV) for the organic fraction of the biomass.

Based on the thermodynamic states of the streams, their corresponding exergy rates can be expressed as:

$$\dot{E}x = \dot{E}x_{ph} + \dot{E}x_{ch} \tag{41}$$

$$\dot{E}x_{ph} = \dot{n}\left[(h - h_0) - T_0(s - s_0)\right] \tag{42}$$

$$\dot{E}x_{ch} = \dot{n}\left[\left(\sum_i x_i ex_{i,0} + RT_0\sum_i x_i \ln x_i\right)\right] \tag{43}$$

where x_i denotes molar fraction and $ex_{i,0}$ standard chemical exergy of species i. For each system component, the exergy efficiency is defined as:

$$\eta_{ex} = \frac{\dot{E}x_{Product}}{\dot{E}x_{Fuel}} \tag{44}$$

To calculate the exergy destruction rate and exergy efficiency of each component in the system, the fuel and product exergy expressions are listed in Table 5.

Economic analysis

In assessing energy systems, thermodynamics assists us to better understand system performance. But that does not tell us anything about economic parameters like installation cost, maintenance cost and the cost of useful outputs. Economic considerations play a key role in evaluating power generation systems and in identifying the best one among multiple systems. The present economic analysis of CHP systems includes the initial capital costs of equipment and the operation and maintenance costs. Note that the fuel cost is not considered since we assume the biomass is a free renewable energy source. In this method, a yearly-based evaluation is conducted for all costs and revenues. The total cost per hour is obtained by the following [30]:

$$\dot{Z}_{tot} = \left(CRF \times \phi \times \sum_k Z_k\right) \Big/ t_{hour} \tag{45}$$

Here, Z is the cost of purchasing equipment as reported in Table 6. This cost is converted to an annual cost with the CRF coefficient:

Table 5 – Fuel and product exergy rates of components.

Component	Fuel exergy rate	Product exergy rate
Gasifier	$\dot{E}x_1 + \dot{E}x_{biomass}$	$\dot{E}x_2$
District heating	$\dot{E}x_4 - \dot{E}x_5$	$\dot{E}x_{DHW,2} - \dot{E}x_{DHW,1}$
Scrubber	$\dot{E}x_6 - \dot{E}x_7$	$\dot{E}x_{CW,2} - \dot{E}x_{CW,1}$
Syngas preheater	$\dot{E}x_3 - \dot{E}x_4$	$\dot{E}x_9 - \dot{E}x_8$
Mixer	$\dot{E}x_9 + \dot{E}x_{12}$	$\dot{E}x_{10}$
SOFC	$\dot{E}x_{10} - \dot{E}x_{11} + \dot{E}x_{22} - \dot{E}x_{23}$	$\dot{W}_{SOFC,stack}$
Afterburner	$\dot{E}x_{13} + \dot{E}x_{23}$	$\dot{E}x_{14}$
Air preheater	$\dot{E}x_{14} - \dot{E}x_{15}$	$\dot{E}x_{22} - \dot{E}x_{21}$
MGT	$\dot{E}x_{15} - \dot{E}x_{16}$	$\dot{W}_{MGT}$
Recuperator	$\dot{E}x_{16} - \dot{E}x_{17}$	$\dot{E}x_{21} - \dot{E}x_{20}$
Air compressor	$\dot{W}_{AC}$	$\dot{E}x_{20} - \dot{E}x_{19}$
HRVG	$\dot{E}x_{17} - \dot{E}x_{18}$	$\dot{E}x_{26} - \dot{E}x_{25}$
ORC turbine	$\dot{E}x_{26} - \dot{E}x_{27}$	$\dot{W}_{T,ORC}$
Condenser	$\dot{E}x_{27} - \dot{E}x_{24}$	$\dot{E}x_{CW,2} - \dot{E}x_{CW,1}$
Pump	$\dot{W}_{P,ORC}$	$\dot{E}x_{25} - \dot{E}x_{24}$

Please cite this article as: Karimi MH et al., Performance assessment and optimization of a biomass-based solid oxide fuel cell and micro gas turbine system integrated with an organic Rankine cycle, International Journal of Hydrogen Energy, https://doi.org/10.1016/j.ijhydene.2019.12.143

Table 6 – Cost function of system components.

Component	Cost function
Gasifier [35]	$Z_{Gasifier} = 1600\ (3600\ \dot{m}_{biomass})^{0.67}$
District heating	$Z_{District\ heating} = 8500 + 409\ (A)^{0.85}$
Scrubber [36]	$Z_{Scrubber} = 8500 + 409\ (A)^{0.85}$
Syngas compressor [35]	$Z_{Syngas\ compressor} = (71.1/0.9 - \eta_{SC})(P_8/P_7)\ln(P_8/P_7)$
Syngas preheater [36]	$Z_{Syngas\ preheater} = 8500 + 409\ (A)^{0.85}$
SOFC [37]	$Z_{SOFC} = A_{act}(2.96T_{cell} - 1907)$
SOFC auxiliaries [37]	$Z_{Aux} = 0.1Z_{SOFC}$
Afterburner [35]	$Z_{AB} = ((46.08\ \dot{m}_{14})/(0.995 - P_{23}/P_{14}))(1+\exp(0.018\ T_{14} - 26.4))$
Air preheater [36]	$Z_{Air\ preheater} = 8500 + 409\ (A)^{0.85}$
MGT [37]	$Z_{MGT} = (-98.328\ln(\dot{W}_{MGT}) + 1318.5)\dot{W}_{MGT}$
Recuperator [36]	$Z_{REC} = 8500 + 409\ (A)^{0.85}$
Air compressor [30]	$Z_{AC} = (71.1/0.9 - \eta_{AC})(P_{20}/P_{19})\ln(P_{20}/P_{19})$
ORC turbine [12]	$Z_{T,ORC} = 4750\ (\dot{W}_{T,ORC})^{0.75}$
HRVG [12]	$Z_{HRVG} = 309.14\ (A)^{0.85}$
Condenser [36]	$Z_{Condensor} = 8500 + 409\ (A)^{0.85}$
Pump [12]	$Z_{P,ORC} = 200(\dot{W}_{P,ORC})^{0.65}$

$$CRF = \frac{i(1+i)^N}{(1+i)^N - 1} \tag{46}$$

where i and N are the interest rate and the number of years of operation of the system. In this study, these values are considered to be 20 years and 12%, respectively [31,32]. The maintenance cost is accounted for by applying the factor ϕ of 1.06 [33]. The annual cost is converted to cost per hour by dividing by t_{hour}, the number of operating hours per year (7500 h) [34].

System optimization

Definition of objective functions

In the present study, the exergy efficiency and total cost rate of the system are considered as the two objective functions. Multi-objective optimization is used to maximize the exergy efficiency and minimize the cost of the entire system. The objective functions can be expressed as follows:

Objective function I: CHP exergy efficiency (to be maximized):

$$\eta_{ex,CHP} = \frac{\dot{W}_{net} + \dot{E}x_{DH}}{\dot{E}x_{biomass}} \tag{47}$$

Objective function II: total cost rate (to be minimized):

$$\dot{C}_{tot} = \dot{Z}_{tot} \tag{48}$$

Design parameters

The design parameters selected for the optimization of the hybrid system are: current density of SOFC, fuel utilization factor, SC isentropic efficiency, ORC turbine isentropic efficiency, HRVG pinch point temperature difference, and recuperator effectiveness. The applicable ranges for the design parameters are given in Table 7.

Table 7 – Design parameters used in system optimization and their ranges.

Design parameter	Range
Current density (A/m^2)	1000–3600
Fuel utilization factor	0.7–0.9
SC isentropic efficiency (%)	70–85
ORC turbine isentropic efficiency (%)	70–85
HRVG pinch point temperature difference (°C)	10–30
Recuperator effectiveness	0.7–0.9

Multi-objective optimization

Most engineering problems have one or many different objectives which are often in conflict. Optimization techniques are important tools for trading off between different objectives of engineering problems. Therefore, in order to achieve an optimal solution, a trade-off should be achieved between the objectives. In problems with more than one objective, the interaction of conflicting goals leads to the generation of a set of solutions which are not dominated by any other solution, the so called the Pareto front, which provides flexibility for choosing an appropriate solution. For complex and nonlinear modeling, as well as a large number of decision variables and multiple objective functions, an evolutionary algorithm is often employed, as it is one of the most suitable methods for optimization. Therefore, in this paper, a multi-objective genetic algorithm is used to achieve optimal solutions. The Evolutionary Genetic Algorithm (GA) provides a semi stochastic search method that emulates natural evolution laws to find an optimal solution of a particular problem. In this method, after generating an initial population of solutions as individuals, a pair of these individuals are randomly selected to generate a future population that has more favorable survival characteristics in nature. By repeating this method for several successive generations, the results approach the optimal solution for the system. In this study, the multi-objective GA tool in the optimization toolbox of MATLAB software is used. In this procedure, design parameters are defined in MATLAB and defined values of these parameters are sent to EES. Then, the calculations of thermoeconomic modeling are carried out in EES and the results are sent to MATLAB. This procedure is repeated for every individual solution. The tuning parameters used in the genetic algorithm are given in Table 8.

Table 8 – Evolutionary algorithm tuning parameters and their values.

Tuning parameter	Value
Population size	200
Maximum number of generations	100
Minimum function tolerance	10^{-5}
Probability of crossover	90%
Probability of mutation	1%
Selection process	Tournament
Tournament size	2

Please cite this article as: Karimi MH et al., Performance assessment and optimization of a biomass-based solid oxide fuel cell and micro gas turbine system integrated with an organic Rankine cycle, International Journal of Hydrogen Energy, https://doi.org/10.1016/j.ijhydene.2019.12.143

Results and discussion

Model validation

The gasifier thermodynamic model is calibrated by comparing its outlet syngas composition with experimental data obtained for several biomasses. As seen in Table 9, the obtained results exhibit good agreement with the experimental data. Moreover, to validate the SOFC model, its voltage and power density at different current densities are compared with experimental data reported by Tao et al. [38]. As seen in Table 10, the SOFC proposed model agrees well with the experimental data.

Modeling results

The proposed system performance is first compared with two preliminary configurations in order to find the expected superiorities. The system components and the corresponding number are as follows:

- System 1: Gasifier, SOFC, hot water generator
- System 2: Gasifier, SOFC, MGT, hot water generator
- System 3: Gasifier, SOFC, MGT, ORC, hot water generator

These arrangements are chosen to determine the effects of making the system complex. System 1 operates at atmospheric pressure while the other systems are pressurized. The input parameters for the simulation are listed in Table 11.

The outputs for the three configurations based on the SOFC-gasifier are given in Table 12. It is seen that by using the MGT in the system, the CHP energy efficiency increases slightly from 79.7% to 79.8%, while the addition of the ORC to this system decreases the CHP efficiency from 79.8% to 55.2%. The reason for this reduction in efficiency can be explained by the fact that all of the exhaust gas energy is utilized for district heating when there is no ORC. However, when an ORC is utilized, only a portion of the input thermal energy is converted to electric power by the ORC, and a significant amount of heat is wasted via the condenser. But, due to more power generation, the use of the ORC increases the CHP electrical efficiency from 46.3% to 50.6%. Since the exergy and energy of shaft work are equal while the exergy of thermal energy is typically less than its energy, the excess generation of power in the ORC results in an increase in the CHP exergy efficiency. By comparing the unit cost of electricity values for the Gasifier + SOFC + DH and Gasifier + SOFC + MGT + ORC + DH systems, it is observed that the recovery of the waste heat for use in power generation is cost effective from an economic point of view. Table 13 shows the thermodynamic parameters and mass flow rates at each node of the proposed hybrid system.

Table 14 shows the exergy destruction rate in each cycle component. It is observed that the highest exergy destruction rate is attributable to the gasifier, in which the processes of drying, pyrolysis, partial oxidation and char reduction occur. One way to reduce the exergy destruction in the gasification reactor is to isolate the drying and pyrolysis steps from the

Table 11 – Input parameters used in system modeling.

Input parameter	Value
Ambient temperature (°C)	25
Ambient pressure (bar)	1.01
Gasifier working temperature (°C)	800
Gasifier working pressure (bar)	1.01
SOFC exit temperature (°C)	800
DC-AC inverter efficiency	95%
SOFC fuel utilization factor	0.85
Afterburner combustion efficiency	98%
Return hot water temperature (°C)	30
Supply hot water temperature (°C)	80

Table 9 – Comparison of syngas composition (in %) for present model and experimental data [39–41], for various feedstock.

Species	Feedstock					
	Rubber wood		Sawdust		Olive leaves	
	Present model	Experimental (Jayah et al. [39])	Present model	Experimental (Altafii et al. [40])	Present model	Experiential (Vera et al. [41])
CH_4	1.63	1.30	2.33	2.31	1.42	1.45
CO	16.8	18.4	24.7	20.1	18.7	21.6
CO_2	12.9	10.6	9.39	12.1	11.7	8.30
H_2	15.9	17.0	18.6	14.0	14.7	20.4
N_2	52.7	52.7	45.0	50.8	53.6	40.9

Table 10 – Comparison of SOFC results for the present model and experimental data [38].

Current density (A/m^2)	Cell voltage (V)		Power density (W/m^2)	
	Present model	Experimental	Present model	Experimental
2000	0.75	0.76	0.15	0.15
3000	0.69	0.68	0.21	0.21
4000	0.64	0.62	0.26	0.26
5000	0.58	0.57	0.29	0.29
6000	0.53	0.52	0.32	0.32

Please cite this article as: Karimi MH et al., Performance assessment and optimization of a biomass-based solid oxide fuel cell and micro gas turbine system integrated with an organic Rankine cycle, International Journal of Hydrogen Energy, https://doi.org/10.1016/j.ijhydene.2019.12.143

Table 12 – Comparison between three configurations studied.

Parameter	Gasifier + SOFC + DH	Gasifier + SOFC + MGT + DH	Gasifier + SOFC + MGT + ORC + DH
CHP energy efficiency (%)[a]	79.7	79.8	55.2
CHP electrical efficiency (%)[b]	32.9	46.3	50.6
CHP exergy efficiency (%)[c]	21.2	31.7	32.8
Cost rate ($/h)	8.50	9.5	10.9
Electricity (kW)	247	347	380
Unit cost of electricity ($/kWh)	0.034	0.027	0.028
Heating capacity (kW)	352	252	34.5
Power to heat ratio	0.70	1.40	11.3

[a] Defined as $\eta_{CHP} = (\dot{Q}_{DH} + \dot{W}_{net})/(\dot{m}_{biomass} LHV_{biomass})$.
[b] Defined as $\eta_{el,CHP} = (\dot{W}_{net})/(\dot{m}_{biomass} LHV_{biomass})$.
[c] Defined as $\eta_{ex,CHP} = (\dot{E}x_{DH} + \dot{W}_{net})/(\dot{E}x_{biomass})$.

partial oxidation and char reduction steps, and to use the syngas heat for drying (instead of burning a part of the biomass). Although the SOFC exergy efficiency is relatively high, this component is the second highest contributor to the system exergy destruction. Table 14 lists the component exergy efficiencies, and reveals that the scrubber performs poorly from a second law standpoint and the afterburner has the highest exergy efficiency.

Parametric analysis

To enhance understanding of system performance, it is useful to examine the effects of variations of major design parameters on system efficiency. In this paper, in order to investigate the system performance in more detail, it is necessary to perform a parametric study. The effect of current density on the voltage and voltage drops is shown in Fig. 3(a). As the current density increases, the hydrogen consumption rate in the electrochemical reaction rises, and the temperature of the SOFC stack increases due to the endothermic nature of the reaction. The simultaneous increase in current density and fuel cell temperature reduces the Nernst voltage and increases the ohmic, activation and concentration voltage drops, so that the fuel cell output voltage decreases. Fig. 3(b) illustrates the effect of current density on the power generation of the SOFC and the MGT, as well as the net power generation. According to Eq. (19), the power generation of the fuel cell is affected by two parameters: current density and output voltage. It is seen that, with increasing current density, the output voltage of the fuel cell decreases. But the effect of voltage reduction is greater than the effect of current density growth and, subsequently, the generated power of the fuel cell declines. Furthermore, increasing the current density does not have a significant effect on the MGT power generation and it remains constant. Therefore, by reducing the power generation of the fuel cell and keeping the power of the micro gas turbine constant, the net power generation decreases with increasing current density.

According to Fig. 3(c), the exergy efficiency decreases with increasing current density. This reduction is due to the decrease in fuel cell voltage in response to a rise in current

Table 13 – Thermodynamic quantities at state points.

State	$\dot{m}$ (kg.s^{-1})	T (K)	P (bar)
1	0.04	298	1.01
2	0.07	298	1.01
3	0.11	1070	1.01
4	0.11	1070	1.00
5	0.11	656	0.998
6	0.11	363	0.993
7	0.11	363	0.988
8	0.11	323	0.983
9	0.11	432	2.51
10	0.11	848	2.51
11	0.34	996	2.50
12	0.36	1070	2.50
13	0.22	1070	2.50
14	0.14	1070	2.50
15	0.71	1150	2.47
16	0.71	1020	2.47
17	0.71	849	1.02
18	0.71	553	1.02
19	0.71	377	1.01
20	0.71	298	1.01
21	0.60	401	2.52
22	0.60	775	2.51
23	0.60	948	2.51
24	0.57	1070	2.50
25	0.24	333	0.52
26	0.24	333	10.0
27	0.24	455	10.0
28	0.24	388	0.52

Table 14 – Exergy efficiencies and exergy destruction rates of the main components of the system.

Component	Exergy efficiency (%)	Exergy destruction rate (kW)
Gasifier	56.2	459
SOFC stack	77.8	135
Afterburner	94.5	26.1
Syngas preheater	78.4	14.4
Recuperator	87.3	13.8
Micro gas turbine	93.7	11.6
HRSG	88.8	6.22
Organic Rankine turbine	87.8	4.76
Syngas compressor	83.4	4.10
Condenser	89.6	1.23
Scrubber	57.2	0.42
District heating	91.1	0.27
Organic Rankine cycle pump	85.1	0.26

Please cite this article as: Karimi MH et al., Performance assessment and optimization of a biomass-based solid oxide fuel cell and micro gas turbine system integrated with an organic Rankine cycle, International Journal of Hydrogen Energy, https://doi.org/10.1016/j.ijhydene.2019.12.143

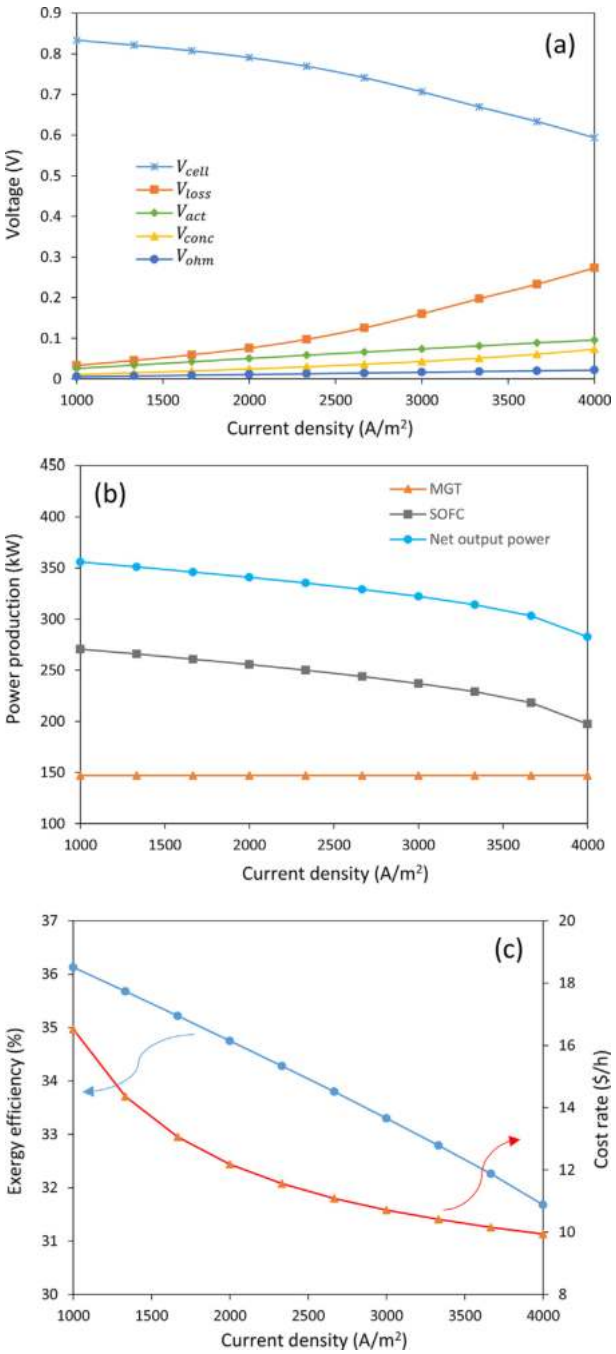

Fig. 3 – Impact of current density on (a) cell voltage and overvoltages, (b) electrical power production and (c) exergy efficiency and cost rate.

density and the consequent reduction in the output power of the SOFC. As the net power generation decreases due to the increased current density, low-capacity subsystems are required, leading to lower cost rate, as shown in Fig. 3(c).

The next important parameter in evaluating the fuel cell-based hybrid fuel is the fuel utilization factor. The effect of this parameter in the range of 0.7–0.9 for the determined current density and inlet temperature is shown in Fig. 4(a). It is seen that, with increasing fuel utilization factor, the power generation of the SOFC increases at first and then reduces, while the power generation of the ORC exhibits a decreasing trend. Increasing the fuel utilization factor leads to a rise in the molar air flow rate to the cathode as well as a reduction in the molar fuel flow rate to the SOFC and a reduction in the Nernst voltage; therefore an optimal value exists for the power generation of the SOFC. This optimum value occurs at a fuel utilization factor of 0.87. However, as this factor increases, less fuel is fed to the afterburner, which reduces the heat input to the ORC and, subsequently, decreases the power generation by the system. In Fig. 4(b), the variation is presented of exergy efficiency and cost rate with fuel utilization factor. As mentioned above, as this factor increases, the fuel input rate and power generation by SOFC are reduced, so it is expected that for an optimum value of the fuel utilization factor, the exergy efficiency would be maximized. In addition, it can be seen that the cost rate increases linearly form 11.7 $/hr to 12.4 $/hr as U_f increases from 0.7 to 0.9.

The variation of fuel cell voltage with the SOFC operating pressure is illustrated in Fig. 5(a). As can be seen, the fuel cell operating voltage rises with increasing operating pressure. This trend can be explained by noting that, by increasing the SOFC operating pressure, the outlet temperature of the MGT reduces and, since the micro gas turbine outlet flow is used for preheating the air entering the fuel cell, the inlet temperature to the SOFC stack decreases. As the temperature of the stack

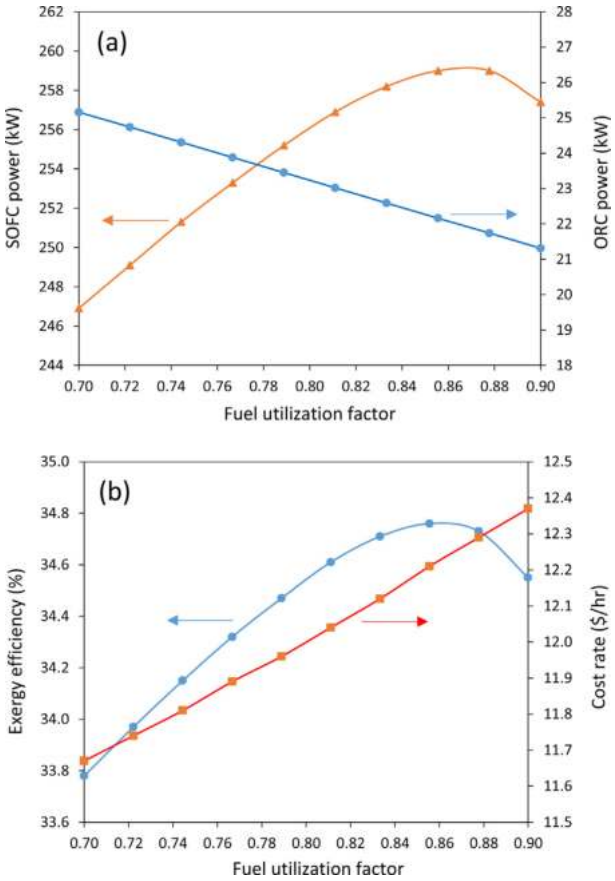

Fig. 4 – Impact of fuel utilization factor on (a) electrical power production and (b) exergy efficiency and cost rate.

Please cite this article as: Karimi MH et al., Performance assessment and optimization of a biomass-based solid oxide fuel cell and micro gas turbine system integrated with an organic Rankine cycle, International Journal of Hydrogen Energy, https://doi.org/10.1016/j.ijhydene.2019.12.143

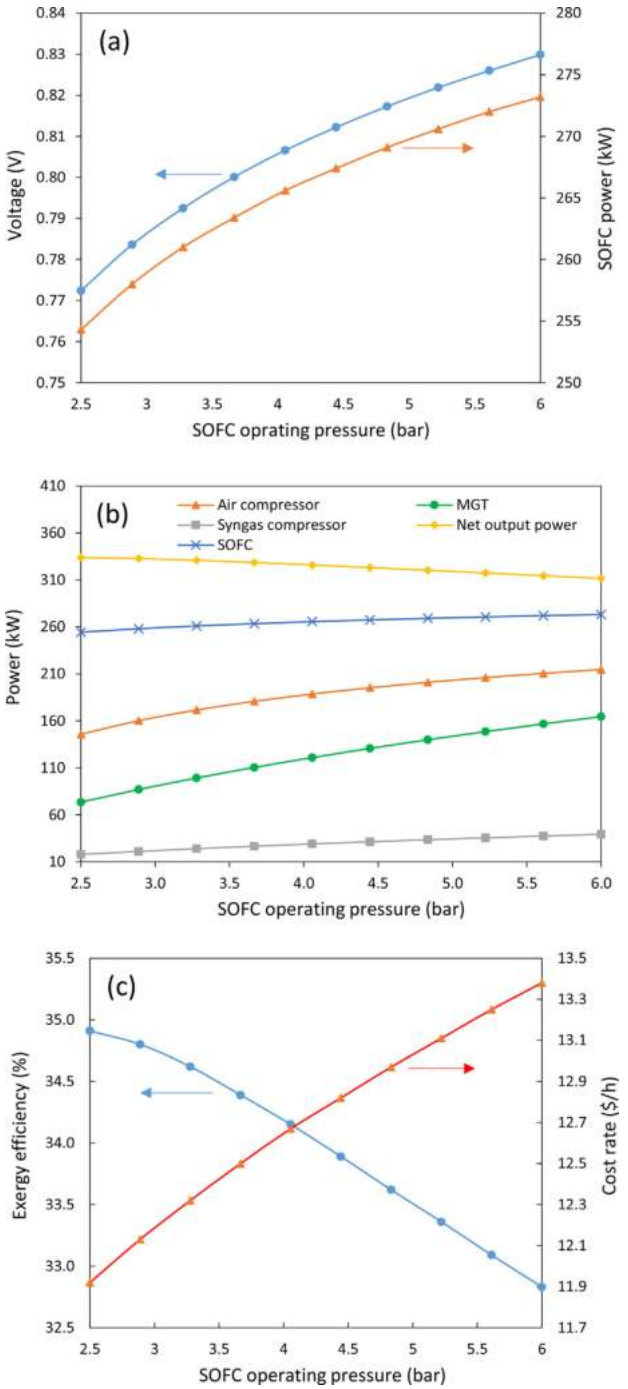

Fig. 5 – Impact of SOFC operating pressure on (a) voltage and overvoltages, (b) electrical power production and (c) exergy efficiency and cost rate.

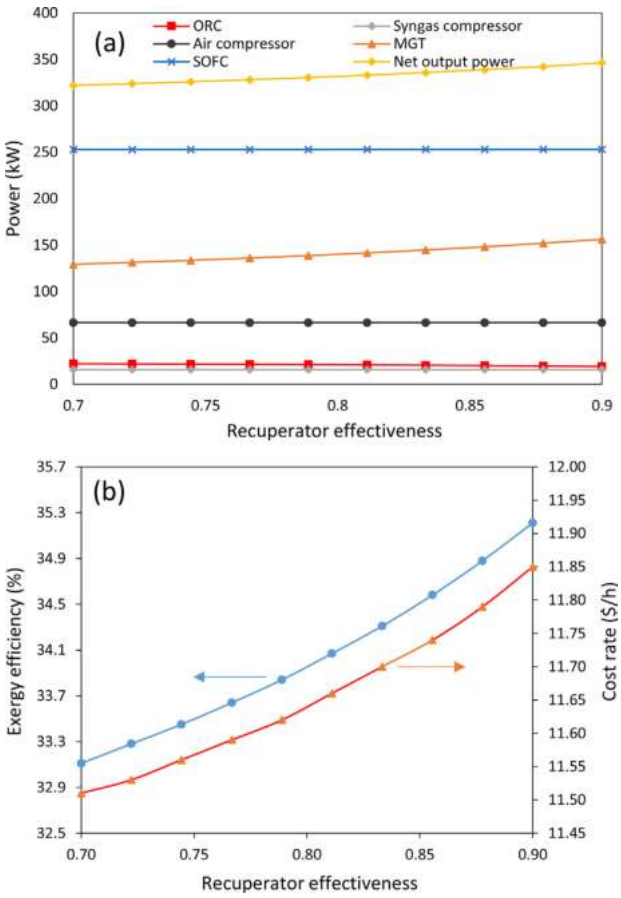

Fig. 6 – Impact of recuperator effectiveness on (a) electrical power production and (b) exergy efficiency and cost rate.

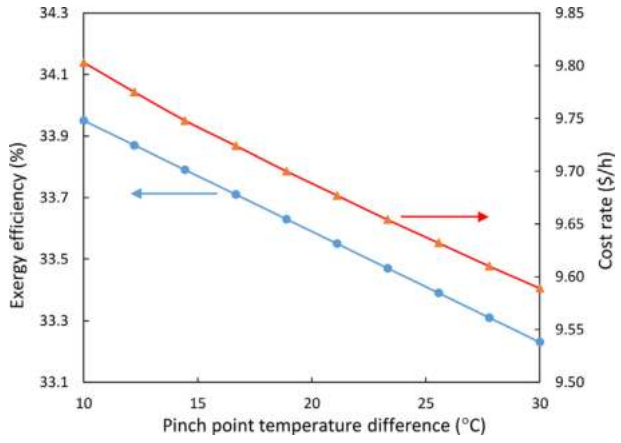

Fig. 7 – Impact of pinch point temperature difference on exergy efficiency and cost rate.

decreases, the Nernst voltage as well as concentration and activation voltage drops increase simultaneously. However, the increase in Nernst voltage is greater than the overvoltage decrease, so the fuel cell voltage increases with an increase in the SOFC operating pressure. Fig. 5(b) shows the effect of SOFC operating pressure on the power generation by the main components, the power consumption of the compressors, and the net power generation of the system. By keeping the current density constant and increasing the SOFC operating pressure, the fuel cell output power increases slightly with increasing voltage. It is clear that the power generation of the micro gas turbine rises considerably as a result of increasing the inlet pressure. In addition, by increasing the fuel cell's

Please cite this article as: Karimi MH et al., Performance assessment and optimization of a biomass-based solid oxide fuel cell and micro gas turbine system integrated with an organic Rankine cycle, International Journal of Hydrogen Energy, https://doi.org/10.1016/j.ijhydene.2019.12.143

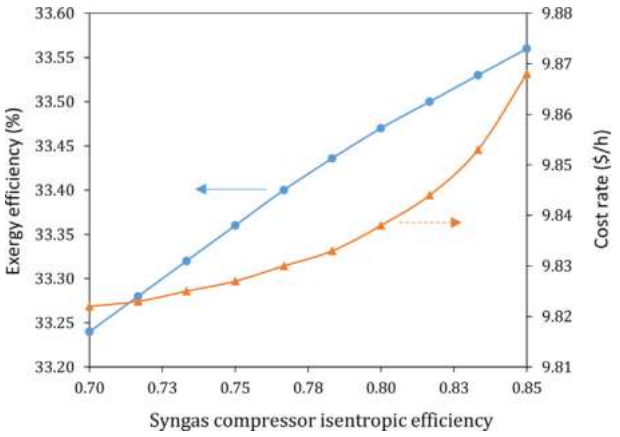

Fig. 8 – Pareto optimal front from multi-objective optimization of the hybrid system.

operating pressure, the power consumption of the compressor increases to provide the required pressure. Although the power generation by the SOFC and MGT increase with increasing pressure, the compressor power consumption increase is greater and leads to a reduction in the net power generation by the system. A reduction in the outlet temperature of the micro gas turbine from increasing the operating pressure of the fuel cell causes the exhaust temperature to the HRSG inlet to decline. By holding the temperature and outlet pressure of the HRSG constant, the heat transfer rate between the hot flow and the ORC working fluid decreases, resulting in a decrease in the mass flow rate in the system, thereby reducing the power generation by the ORC turbine. The variation of exergy efficiency with fuel cell operating pressure is shown in Fig. 5(c). Since the fuel cell's operating pressure does not affect the molar flow rate of the inlet fuel and thus the inlet exergy rate to the system, the exergy efficiency is regarded as a function of net power generation. Therefore, the exergy efficiency declines with decreasing net power generation. But with increasing SOFC pressure, larger and more expensive compressors and gas turbines are required, which leads to higher system costs.

The effect of the recuperator efficiency on the power production of the various components is shown in Fig. 6(a). It is observed that, with increasing recuperator efficiency, the outlet temperature (T_{21}) is increased and approaches the turbine outlet temperature. Therefore, the inlet temperature to the fuel cell cathode also increases. By increasing the inlet temperature to the SOFC, the activation and concentration voltage drops increase and the Ohmic voltage drop decreases, which results in the fuel cell voltage remaining constant. As a result, the power generation by the SOFC remains constant as the efficiency of the recuperator is modified. However, with increasing SOFC inlet temperature, the exhaust gases enter the MGT at higher temperatures. As a result, increasing the efficiency of the recuperator augments the power generation of the MGT and reduces the outlet temperature of the micro gas turbine. The result is a reduction of the inlet thermal energy to the ORC as well as a reduction in the power generation by the cycle. Increasing the power generation in the MGT increases the net power generation. The effect of recuperator efficiency on the exergy efficiency and cost rates is shown in Fig. 6(b). Increasing the net power generation by the hybrid system for the same inlet exergy causes the exergy efficiency of the system to increase. Additionally, with increasing recuperator efficiency, more area is required for heat transfer, which in turn increases system costs. The increase in system cost rates is also depicted in Fig. 6(b).

As shown in Fig. 7, the lowest exergy efficiency and ORC cost rate are associated with the highest pinch point temperature difference. By keeping the inlet pressure of the ORC turbine constant, increasing the pinch point temperature difference results in an increase in the temperature of the outlet hot flow and thus reduces the heat transfer rate in the HRVG and the inlet exergy rate to the ORC. Moreover, reducing the heat transfer rate reduces the mass flow rate through and power generation by the turbine. Reducing the power generation leads to a decrease in the exergy efficiency by increasing the pinch point temperature difference. So reducing the heat transfer rate by increasing the ΔT_{Pinch} causes the required area for heat transfer to decline, which decreases the costs related to the heat exchanger. This is the main reason for cost rate reduction with increasing ΔT_{Pinch}.

Fig. 8 shows the effect of a change in syngas compressor isentropic efficiency on the exergy efficiency and the cost rate. An increase in the syngas compressor isentropic efficiency reduces the power required by this device and subsequently increases the net power produced by the MGT. Therefore, this changes improves the system exergy efficiency. But, a compressor with a higher isentropic efficiency normally costs more.

Fig. 9 shows the impact of air compressor isentropic efficiency on the exergy efficiency and the cost rate. As shown in Fig. 9, utilizing an air compressor with a higher isentropic efficiency, in addition to reducing its input power, less energy is supplied to the ORC which causes a decline in the ORC cycle power production. On the whole, the reduction in power required by the air compressor exceeds the reduction in ORC power production, so the system exergy efficiency increases. This also leads to a decrease in system cost rate.

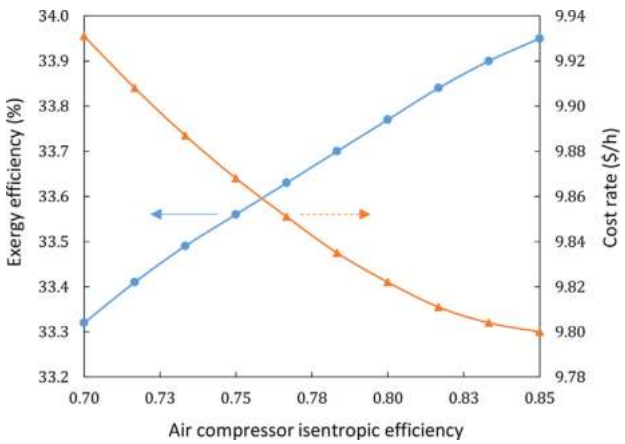

Fig. 9 – Distribution of design parameters at optimum point B.

Please cite this article as: Karimi MH et al., Performance assessment and optimization of a biomass-based solid oxide fuel cell and micro gas turbine system integrated with an organic Rankine cycle, International Journal of Hydrogen Energy, https://doi.org/10.1016/j.ijhydene.2019.12.143

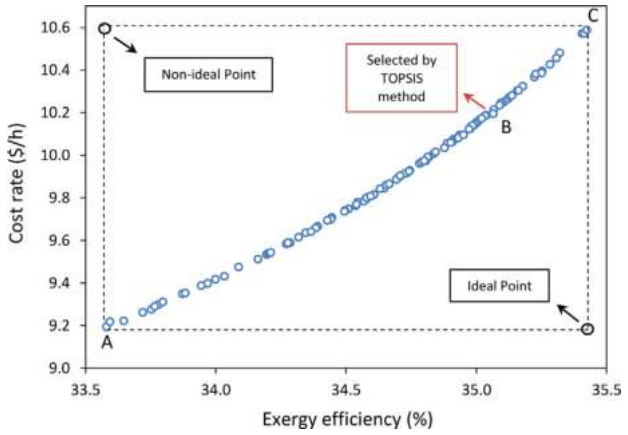

Fig. 10 – Impact of syngas compressor isentropic efficiency on exergy efficiency and cost rate.

Optimization results

It can be observed in the previous section that varying some parameters increases both the system exergy efficiency and cost rate. As can be seen in Fig. 10, which shows the Pareto front, the system cost rate always increases with increasing exergy efficiency. All of the points on the Pareto front are related to the optimal conditions of the system and are not dominated by other functional points. Point C is the optimal condition when only the exergy efficiency is considered as the objective function and the value of the exergy efficiency at this point is 35.4%. If the goal is to minimize only system cost, then point A is the ideal point and the cost rate at this point is 9.21 $/hr.

The TOPSIS method is used to determine the best practical point on the Pareto front. In this method, the ideal point is assumed to be a point in which both objective functions have

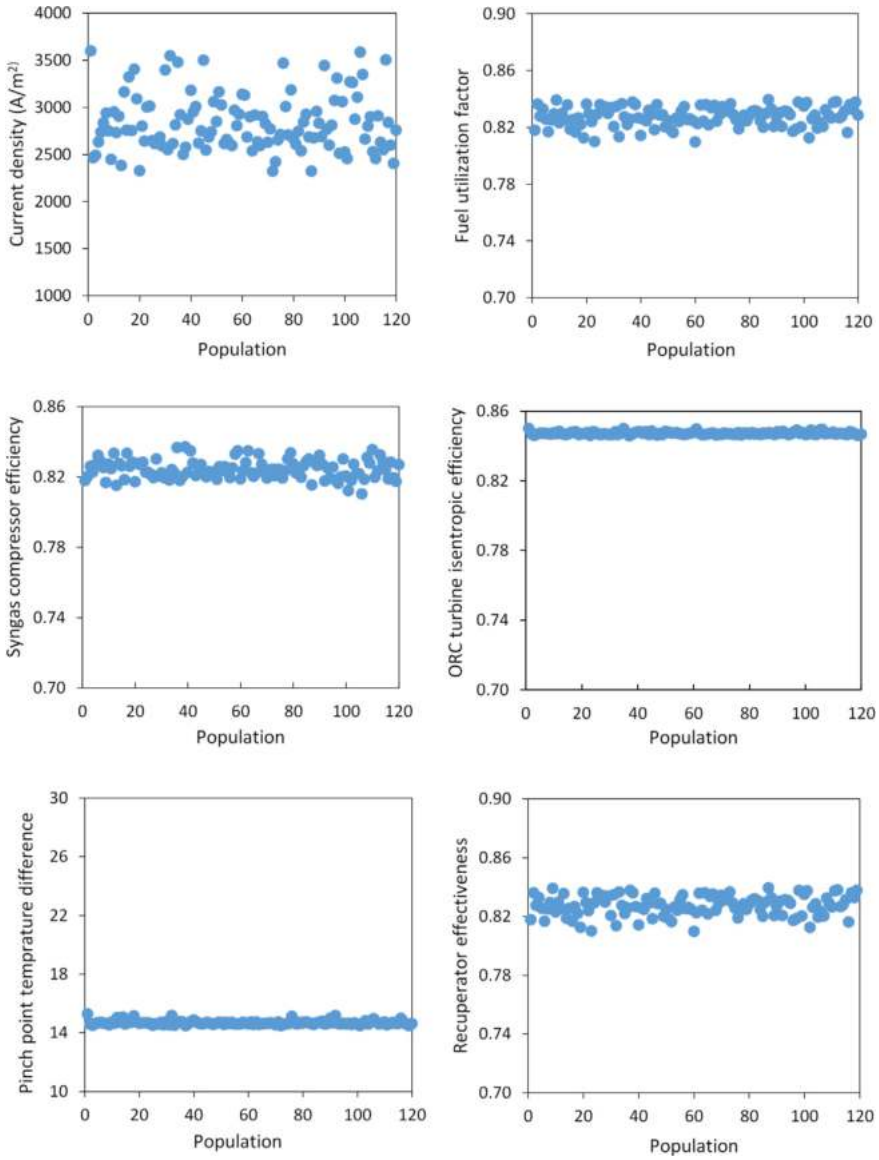

Fig. 11 – Impact of air compressor isentropic efficiency on exergy efficiency and cost rate.

Please cite this article as: Karimi MH et al., Performance assessment and optimization of a biomass-based solid oxide fuel cell and micro gas turbine system integrated with an organic Rankine cycle, International Journal of Hydrogen Energy, https://doi.org/10.1016/j.ijhydene.2019.12.143

Table 15 – Values of design parameters at points A, B and C.

Design parameter	A	B	C
i (A/m^2)	2320	2590	3600
U_f	0.84	0.84	0.82
η_{SC}	0.82	0.83	0.82
$\eta_{ORC,T}$	0.85	0.85	0.85
ΔT_{Pinch}	14.8	14.6	15.3
ε_{REC}	0.84	0.86	0.82

their best values, and also the non-ideal point is considered to be a point in which the objective functions have their worst values. The best point is then selected, which has the least distance from the ideal point and the maximum distance from the non-ideal point. Finally, point B is obtained in Fig. 10 as the best point for the desired problem. This has an exergy efficiency of 35.1% and a cost rate of 10.2 $/hr with the capability for generating 329 kW of electricity and 56 kW of heating. The values of design parameters for each of points A, B and C are given in Table 15.

To clarify the changes of design parameters during optimization, the dispersion graph of each of these parameters is shown in Fig. 11. The results show that the ORC turbine isentropic efficiency tends to become as maximal as possible. The pinch point temperature difference tends to remain at a constant value. Among the parameters, the current density has the highest distribution within its defined interval, while the other parameters are relatively concentrated within a certain range. This suggests that the current density has the greatest effect on the conflict between the two objective functions.

Case study

The power generation capacity by the optimized system from the total amount of Iran rice straw produced in one year is presented in Table 16. In this calculation, changes in parameter values when shifting from a small scale to a large scale power plant are neglected. Until now it is observed that the system can efficiently generate power from rice straw; but note also that as mentioned before this residue is bulky and its collection requires much energy. Thus power generation from rice straw is a suitable practice when the system output power compensates for the energy consumption for gathering this feedstock. In 2012, Nguyen et al. [42] performed a study about the energy needed for rice straw collection. They considered two scenarios, one conventional, by manpower and the other mechanical, by using machinery, and calculated the energy demand for each scenario. They showed that on average about 4500 MJ/ton energy is needed for rice straw collection.

Table 16 – Case study results.

Parameter	Value
Iran rice straw annual production (ton)	3,520,000
Electrical energy capacity (GWh)	6660
Thermal energy capacity (GWh)	1140
Total energy harvested (MJ/ton)	7990

With this result it is observed that the system proposed here, with 7990 MJ/ton output energy, leads to positive energy balance of about 80% over the input energy for gathering the feedstock.

Conclusion

A comprehensive investigation of a biomass-based CHP system is carried out, considering Iran rice straw as the gasifier feedstock. The system key features are compared with preliminary configurations. The effects on system performance are studied of various parameters: current density, fuel utilization factor, SOFC working pressure, pinch point temperature difference, recuperator effectiveness and turbomachinery isentropic efficiency. The major findings of the parametric study are as follows: the current density has the greatest effect on the exergy efficiency and cost rate; by increasing the fuel utilization factor, although the SOFC output power increases, the afterburner outlet temperature decreases, leading to a reduction in ORC power generation; raising the SOFC working pressure increases the compressor power demand and the system cost rate and but decreases the exergy efficiency; raising the recuperator effectiveness increases the MGT and subsequently the system net power output, even though this reduces the ORC power generation; and increasing the pinch point temperature difference leads to a decrease in system exergy efficiency and cost.

Through a multi-objective optimization a compromise between exergy efficiency and cost rate is made. At the optimum scenario the system has an exergy efficiency of 35.1% with a 10.2 $/h cost rate. The exergy analysis reveals that the greatest irreversibility occurs in the gasifier. This means that for such a system the main focus should be on decreasing the irreversibility within the gasifier prior to adding a new bottoming cycle for improving efficiency. However, the ORC cycle in the present configuration increases the exergy efficiency relative to similar systems. The electrical and thermal energy capacities from Iranian rice straw by the optimized system are 6660 GWh and 1140 GWh, respectively. By comparing its output energy with the energy demand for rice straw collection, it is concluded that the proposed system can achieve a positive energy balance.

REFERENCES

[1] Dincer I, Marc AR, Ahmadi P. Optimization of Energy Systems. New York: Wiley; 2017.
[2] Ahmadi P. Environmental impacts and behavioral drivers of deep decarbonization for transportation through electric vehicles. J Clean Prod 2019;225:1209–19. https://doi.org/10.1016/j.jclepro.2019.03.334.
[3] Mao G, Zou H, Chen G, Du H, Zuo J. Past, current and future of biomass energy research: a bibliometric analysis. Renew Sustain Energy Rev 2015;52:1823–33.
[4] Kapoor M, Panwar D, Kaira GS. Bioprocesses for enzyme production using agro-industrial wastes: technical

Please cite this article as: Karimi MH et al., Performance assessment and optimization of a biomass-based solid oxide fuel cell and micro gas turbine system integrated with an organic Rankine cycle, International Journal of Hydrogen Energy, https://doi.org/10.1016/j.ijhydene.2019.12.143

challenges and commercialization potential. Agro-Ind Wastes Feed Enzym Prod 2016:61–93.
[5] Satlewal A, Agrawal R, Bhagia S, Das P, Ragauskas AJ. Rice straw as a feedstock for biofuels: availability, recalcitrance, and chemical properties. Biofuels Bioprod Biorefining 2018;12:83–107.
[6] Safari F, Tavasoli A, Ataei A. Gasification of sugarcane bagasse in supercritical water media for combined hydrogen and power production: a novel approach. Int J Environ Sci Technol 2016;13:2393–400.
[7] Chitgar N, Emadi MA, Chitsaz A, Rosen MA. Investigation of a novel multigeneration system driven by a SOFC for electricity and fresh water production. Energy Convers Manag 2019;196:296–310.
[8] Bang-Møller C, Rokni M. Thermodynamic performance study of biomass gasification, solid oxide fuel cell and micro gas turbine hybrid systems. Energy Convers Manag 2010;51:2330–9.
[9] Alderucci V, Antonucci PL, Maggio G, Giordano N, Antonucci V. Thermodynamic analysis of SOFC fuelled by biomass-derived gas. Int J Hydrogen Energy 1994;19:369–76.
[10] Omosun AO, Bauen A, Brandon NP, Adjiman CS, Hart D. Modelling system efficiencies and costs of two biomass-fuelled SOFC systems. J Power Sources 2004;131:96–106.
[11] Razmi AR, Janbaz M. Exergoeconomic assessment with reliability consideration of a green cogeneration system based on compressed air energy storage (CAES). Energy 2020;204. https://doi.org/10.1016/j.enconman.2019.112320.
[12] Emadi MA, Chitgar N, Oyewunmi OA, Markides CN. Working-fluid selection and thermoeconomic optimisation of a combined cycle cogeneration dual-loop organic Rankine cycle (ORC) system for solid oxide fuel cell (SOFC) waste heat recovery. Appl Energy 2020. https://doi.org/10.1016/j.apenergy.2019.114384. In press.
[14] Bang-Møller C, Rokni M, Elmegaard B. Exergy analysis and optimization of a biomass gasification, solid oxide fuel cell and micro gas turbine hybrid system. Energy 2011;36:4740–52.
[15] Rokni M. Biomass gasification integrated with a solid oxide fuel cell and Stirling engine. Energy 2014;77:6–18.
[16] Morandin M, Maréchal F, Giacomini S. Synthesis and thermo-economic design optimization of wood-gasifier-SOFC systems for small scale applications. Biomass Bioenergy 2013;49:299–314.
[17] Emadi MA, Mahmoudimehr J. Modeling and thermo-economic optimization of a new multi-generation system with geothermal heat source and LNG heat sink. Energy Convers Manag 2019;189:153–66.
[18] Razmi A, Soltani M, Torabi M. Investigation of an efficient and environmentally-friendly CCHP system based on CAES, ORC and compression-absorption refrigeration cycle: energy and exergy analysis. Energy Convers Manag 2019;195:1199–211.
[19] Pierobon L, Rokni M, Larsen U, Haglind F. Thermodynamic analysis of an integrated gasification solid oxide fuel cell plant combined with an organic Rankine cycle. Renew Energy 2013;60:226–34.
[20] Yan Z, Zhao P, Wang J, Dai Y. Thermodynamic analysis of an SOFC-GT-ORC integrated power system with liquefied natural gas as heat sink. Int J Hydrogen Energy 2013;38:3352–63.
[21] Ebrahimi M, Moradpoor I. Combined solid oxide fuel cell, micro-gas turbine and organic Rankine cycle for power generation (SOFC–MGT–ORC). Energy Convers Manag 2016;116:120–33.
[22] Eveloy V, Karunkeyoon W, Rodgers P, Al Alili A. Energy, exergy and economic analysis of an integrated solid oxide fuel cell–gas turbine–organic Rankine power generation system. Int J Hydrogen Energy 2016;41:13843–58.
[23] Tan L, Dong X, Gong Z, Wang M. Investigation on performance of an integrated SOFC-GE-KC power generation system using gaseous fuel from biomass gasification. Renew Energy 2017;107:448–61.
[24] Ministry of Agriculture - Jahadn.d. https://www.maj.ir/ (accessed March 18, 2019).
[25] Oladosu Y, Rafii MY, Abdullah N, Magaji U, Hussin G, Ramli A, Miah G. Fermentation quality and additives: a case of rice straw silage. BioMed Res Int 2016;2016:1–14.
[26] Jarungthammachote S, Dutta A. Thermodynamic equilibrium model and second law analysis of a downdraft waste gasifier. Energy 2007;32:1660–9.
[27] Salimi M, Nejati B, Karimi A, Tavasoli A. Hydrothermal gasification performance of Iranian rice straw in supercritical water media for hydrogen-rich gas production. BioResources 2016;11:6362–77.
[28] Moghimi M, Emadi M, Mirzazade Akbarpoor A, Mollaei M. Energy and exergy investigation of a combined cooling, heating, power generation, and seawater desalination system. Appl Therm Eng 2018;140:814–27.
[29] Kotas TJ. The exergy method of thermal plant analysis. Elsevier; 2013.
[30] Bejan A, Tsatsaronis G, Moran M. Thermal design and optimization. John Wiley & Sons; 1996.
[31] Javan S, Mohamadi V, Ahmadi P, Hanafizadeh P. Fluid selection optimization of a combined cooling, heating and power (CCHP) system for residential applications. Energy Convers Manag 2016;96:26–38.
[32] Sanaye S, Emadi M, Refahi A. Thermal and economic modeling and optimization of a novel combined ejector refrigeration cycle. Int J Refrig 2019;98:480–93.
[33] Abbasi HR, Pourrahmani H, Yavarinasab A, Emadi MA, Hoorfar M. Exergoeconomic optimization of a solar driven system with reverse osmosis desalination unit and phase change material thermal energy storages. Energy Convers Manag 2019;199:112042.
[34] Moghimi M, Emadi M, Ahmadi P, Moghadasi H. 4E analysis and multi-objective optimization of a CCHP cycle based on gas turbine and ejector refrigeration. Appl Therm Eng 2018;141:516–30.
[35] Khanmohammadi S, Atashkari K, Kouhikamali R. Exergoeconomic multi-objective optimization of an externally fired gas turbine integrated with a biomass gasifier. Appl Therm Eng 2015;91:848–59.
[36] Ahmadi P, Dincer I, Rosen MA. Exergy, exergoeconomic and environmental analyses and evolutionary algorithm based multi-objective optimization of combined cycle power plants. Energy 2011;36(10):5886–98.
[37] Calise F, d'Accadia MD, Vanoli L, Von Spakovsky MR. Single-level optimization of a hybrid SOFC–GT power plant. J Power Sources 2006;159:1169–85.
[38] Tao G, Armstrong T, Virkar A. Intermediate temperature solid oxide fuel cell (IT-SOFC) research and development activities at MSRI. In: Ninet. Annu. ACERC&ICES Conf.; 2005.
[39] Jayah TH, Aye L, Fuller RJ, Stewart DF. Computer simulation of a downdraft wood gasifier for tea drying. Biomass Bioenergy 2003;25:459–69.
[40] Altafini CR, Wander PR, Barreto RM. Prediction of the working parameters of a wood waste gasifier through an equilibrium model. Energy Convers Manag 2003;44:2763–77.
[41] Vera D, de Mena B, Jurado F, Schories G. Study of a downdraft gasifier and gas engine fueled with olive oil industry wastes. Appl Therm Eng 2013;51:119–29.
[42] Nguyen VH, Topno S, Balingbing C, Nguyen VCN, Röder M, Quilty J, Jamieson C, Thornley P, Gummert M. Generating a positive energy balance from using rice straw for anaerobic digestion. Energy Rep 2016;2:117–22.

Please cite this article as: Karimi MH et al., Performance assessment and optimization of a biomass-based solid oxide fuel cell and micro gas turbine system integrated with an organic Rankine cycle, International Journal of Hydrogen Energy, https://doi.org/10.1016/j.ijhydene.2019.12.143